inorganics

MDPI

Article

Central-to-Helical-to-Axial Chirality Transfer in Chiroptical Sensing with Ferrocene Chromophore

Marko Nuskol [1], Petar Šutalo [2], Monika Kovačević [1], Ivan Kodrin [2,*] and Mojca Čakić Semenčić [1,*]

[1] Department of Chemistry and Biochemistry, Faculty of Food Technology and Biotechnology, University of Zagreb, Pierottijeva 6, 10000 Zagreb, Croatia; mnuskol@pbf.unizg.hr (M.N.); mkovacevic@pbf.unizg.hr (M.K.)
[2] Department of Chemistry Faculty of Science, University of Zagreb, Horvatovac 102a, 10000 Zagreb, Croatia; psutalo@chem.pmf.hr
* Correspondence: ikodrin@chem.pmf.hr (I.K.); mojca.cakic@pbf.unizg.hr (M.Č.S.); Tel.: +385-1-4606-403 (I.K.); +385-1-4605-067 (M.Č.S.)

Abstract: The effect of attaching the achiral, cyclic 1-aminocyclohexanecarboxylic acid (Ac6c) directly to the aminoferrocene unit (Ac6c−NH−Fc) appears to be a promising route for the development of a new chiroptical sensor based on a ferrocene chromophore. Three new compounds (Boc−AA−Ac6c−NH−Fc; AA = L-Ala, L-Val, L-Phe) were synthesized, spectroscopically characterized (IR, NMR, CD), and conformationally analyzed (DFT). The chiral information was transferred from the L-amino acid to the ferrocene chromophore by the predominant formation of *P*-helical structures with ten-membered hydrogen-bonded rings (β-turns). The perturbation of the ferrocene chromophore and the appearance of the negative CD signal near 470 nm originates from a relative orientation of the directly linked amide and cyclopentadienyl planes, described by the dihedral angle χ. The sterically demanding Ac6c amino acid makes *trans*-like configurations more favorable and thus restricts the dihedral angle χ, which then leads to the appearance of the negative peak near 470 nm in the CD curve.

Keywords: circular dichroism (CD); density functional theory (DFT); conformational analysis; ferrocene peptides; chirality

Citation: Nuskol, M.; Šutalo, P.; Kovačević, M.; Kodrin, I.; Čakić Semenčić, M. Central-to-Helical-to-Axial Chirality Transfer in Chiroptical Sensing with Ferrocene Chromophore. *Inorganics* **2023**, *11*, 225. https://doi.org/10.3390/inorganics11060225

Academic Editor: Rainer Winter

Received: 9 May 2023
Revised: 22 May 2023
Accepted: 23 May 2023
Published: 24 May 2023

1. Introduction

Chiroptical spectroscopic methods such as optical rotational dispersion (ORD), electronic circular dichroism (ECD), vibrational circular dichroism (VCD), and optical Raman activity (ROA) are powerful tools for the stereochemical structural elucidation of chiral molecules [1]. However, due to the lack of strong chromophores, large specific rotation requirements, and high sample concentration requirements, the absolute configuration of many chiral molecules cannot be directly determined using chiroptical responses [2]. One of the main issues in determining absolute configuration with ECD are signals of negligible intensity, which typically occur at low wavelengths in the region of other absorbing chromophores, impurities, and solvents [3]. This problem can be overcome by using achiral probes that have chromophores and can be covalently or non-covalently bound to chiral analytes to give rise to noticeable Cotton effects [4–6]. Over the past decade, Wolf and his group have made one of the largest contributions to the development of chiroptical probes (Figure 1) that can be used to differentiate the chirality of molecules and for the quantitative determination of optical purity [7–14]. For example, aminoborane has been successfully used as a CD probe to determine the concentration, absolute configuration, and enantiomeric excess of alcohols, amino alcohols, and diols [13]. The covalent binding of chiral amines to achiral (pseudo)halogenated quinones induced signals in CD spectra that allowed the determination of the absolute configuration and quantification of the enantiomeric ratio [15]. In addition, late transition metal complexes have been used for terpene and terpenoid sensing [10]; aryl fluoride probes for chiroptical analysis of amino acids,

biothiols, amines, and amino alcohols [7]; metal salts for qualitative chirality sensing of unprotected amino acids, hydroxy acids, amino alcohols, amines, and carboxylic acids [12], etc. All previously described optical sensors provide strong CD responses above 300 nm, which precludes possible interference with other CD-active species.

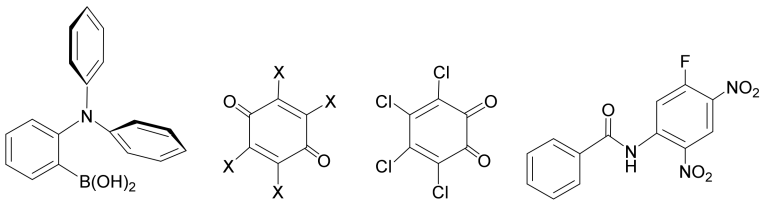

Figure 1. Examples of CD probes developed by Wolf and coworkers (X = F, Cl, CN).

Ferrocene is an exceptional organometallic complex used by many researchers for various applications and investigations [16]. In the absence of chiral perturbation, e.g., covalent binding of chiral ligands [17], interaction with chiral hosts [18], supramolecular assembly [19], etc., this inherently achiral chromophore is CD-silent. However, when embedded in a chiral environment, it exhibits Cotton effects in the visible region (at about 470 nm) of the CD spectrum. In the last 30 years, many bioconjugates have been prepared from ferrocene, which serves as a molecular scaffold and regulates conformation through intramolecular hydrogen bonding (IHB) and amino acids to mimic the secondary structure of natural peptides [20–24]. These derivatives are often characterized by a strong CD activity due to the locking of the ferrocene moiety into a *P*- or *M*-helical conformation by IHBs between the pod and peptide chains. Several years ago, our group began studying dipeptide derivatives of aminoferrocene [25–27] and found that the transfer of chiral information from the folded peptide sequence to the ferrocene chromophore results in signals in the visible region of the CD spectra of these bioconjugates. Negative bands were observed in the spectra of homochiral peptides containing L-amino acids that prefer right-handed β-turn geometries and vice versa. Using a combined experimental and theoretical approach, we recently found that the origin of these Cotton effects lies in the deviation from coplanarity of the cyclopentadienyl ring and the directly connected amide plane caused by intrachain hydrogen bonding [28]. In addition, we found a correlation between the sign of the CD curve near 470 nm and the sign of the dihedral angle (χ) describing this deviation; namely, positive values of χ coincide with the positive signals and negative values with the negative signals (Figure 2). The ferrocene moiety in conformationally flexible peptides can adopt both *cis*-like and *trans*-like orientations relative to the peptide segment, leading to opposite values of the χ-angle and thus the sign of the CD spectra. Therefore, we could not readily correlate the sign of the CD curve with the helicity of the peptide sequence, which in turn depends on the chirality of the backbone residues.

Continuing our research [29], we prepared aminoferrocene-derived peptides Boc−L−Ala−$(Aib)_n$−NHFc (n = 1–3) containing repeating units of the helicogenic achiral α-aminoisobutyric acid (Aib) known to promote β-turn and 3_{10} helical structures [30–32]. We hoped that the *N*-terminal L-Ala would induce a predominant right-handed turn (n = 1) or *P*-helical conformation (n = 2, 3) in the *trans*-like position to avoid the additional steric hindrance, thus limiting the conformational space and allowing a direct correlation between the chirality of the *N*-terminus and the sign of the CD band at around 470 nm. Spectroscopic analysis in conjunction with DFT calculations revealed that the peptide Boc-L-Ala-Aib-NHFc occupies energetically close right-handed conformations that differ in the orientation (*cis*- and *trans*-) of the turn structure with respect to ferrocene, making the experimental correlation between CD signal and chirality of the *N*-terminus impossible. In contrast, Boc−L−Ala−$(Aib)_3$−NHFc was found predominantly in the *trans*-like orientation of the *P*-helical peptide sequence relative to ferrocene. Although the conformational homogeneity of the peptide containing the $(Aib)_3$ sequence allowed for correlation between the chirality of the *N*-terminus (L-) and the CD signal (negative), the extremely challenging condensa-

tion of multiple Aib residues reduces the potential of using $(Aib)_3$−NHFc as a chiral sensor. In pursuit of developing a practical CD sensor, in the present work, we replaced $(Aib)_n$ with its cyclic analogue, 1-aminocyclohexanecarboxylic acid (Ac6c), and investigated the potential of Ac6c−NH−Fc as a chiral sensor. We expected that the sterically demanding Ac6c, coupled with L-amino acids, would reduce the conformational space of the derived dipeptides by forcing the right-handed turn-like substituent into the *trans*-like orientation relative to the second cyclopentadienyl ring of the ferrocene. To determine whether central-to-axial chirality induction in Boc−AA−Ac6c−NH−Fc (AA = L-Ala, L-Val, L-Phe) leads to a clear correlation between the experimentally determined sign of the CD signal and the chirality of the amino acids, we used a combined spectroscopic and theoretical approach.

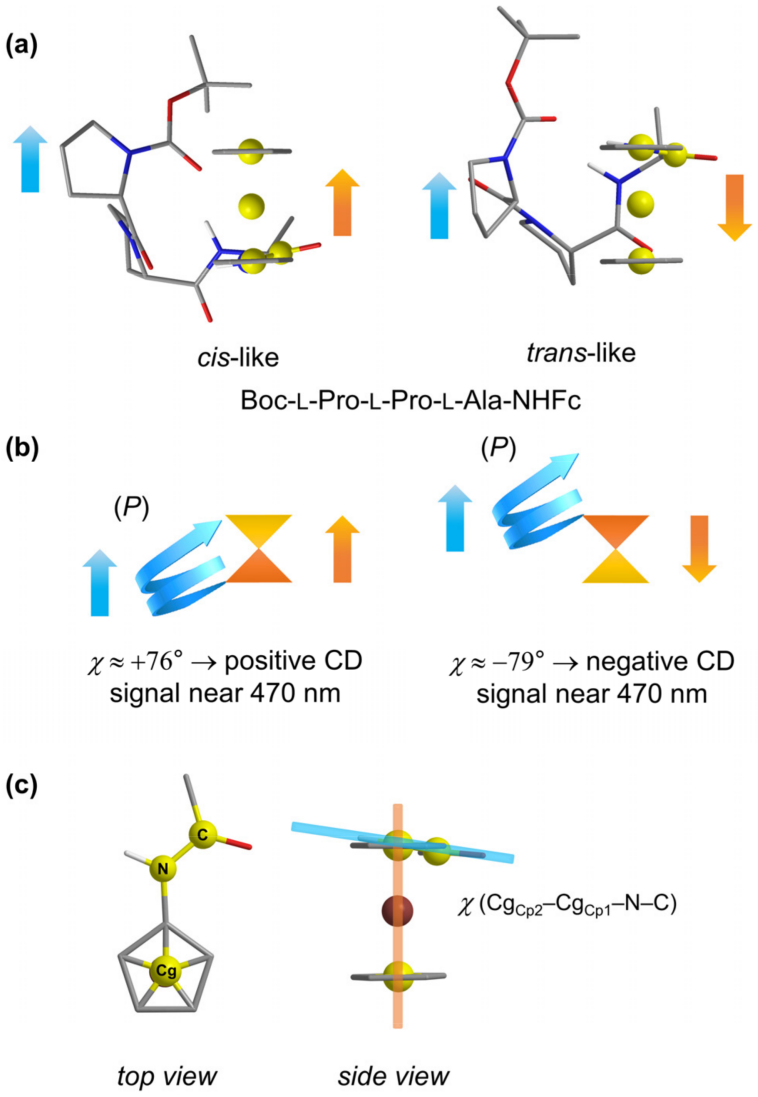

Figure 2. (**a**) Two conformers of Boc-L-Pro-L-Pro-L-Pro-NHFc showing two relative orientations (*cis*-like and *trans*-like) of the ferrocene unit (orange arrow) and the attached (*P*)-helical peptide segment (blue arrow). (**b**) Schematic representations of *cis*-like and *trans*-like relative orientations in which the sign of the ferrocene chromophore observed near 470 nm in the CD spectrum is nicely correlated with the sign of the χ-angle. (**c**) χ-angle is a dihedral angle defined by four atoms, Cg_{Cp}−Cg_{Cp1}−N−C (Cg is a cyclopentadienyl ring centroid), the figure shows a negative χ-angle.

2. Results and Discussion

The targeted compound Boc−Ac6c−NH−Fc (**2**) was synthesized in a 91% yield by HOBt/EDC-mediated coupling of aminoferrocene, obtained by deprotection of Boc−NHFc

(**1**) [33] with Boc−Ac6c−OH (Scheme 1). Target dipeptides **3–5** were synthesized using the procedure described in [34]. Coupling of *N*-deprotected **2** with HOBt/EDC-activated Boc−AA−OH in acetonitrile at an elevated temperature (65 °C) gave **3** (79%), **4** (68%), and **5** (72%), respectively. All signals in the ^{1}H and ^{13}C NMR of **2–5** are registered at their expected positions (Figures S1–S8) and assigned using two-dimensional correlation spectroscopy (NOESY, COSY, HSQC, HMBC) and coupling patterns.

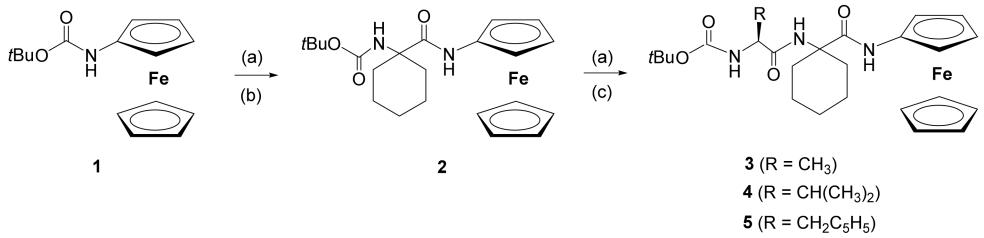

Scheme 1. Syntheses of derivatives **2–5**: (**a**) HCl(*g*)/EtOAc; (**b**) 1. HOBt/EDC, CH_2Cl_2; 2. Boc−Ac6c−OH, CH_2Cl_2; (**c**) 1. HOBt/EDC, MeCN; 2. Boc−AA−OH.

2.1. Infrared (IR) and NMR Studies

Considering the number of IHB donors and acceptors in derivatives **3–5** and the limited conformational flexibility of Ac6c that promotes ten-membered IHB rings [35,36] in the first part of our research, we wanted to determine experimentally whether the β-turn conformation dominates, as in similar dipeptide derivatives of aminoferrocene [25–27,29]. The NH region of IR spectra of dilute solutions of chiral dipeptides **3–5**, shown in Figure 3, contains two distinct stretching bands assigned to hydrogen-bonded (below 3400 cm^{-1}) and IHB-free NH groups (above 3400 cm^{-1}). The intensity of the first band is somewhat weaker, which can be explained by the fact that only one of the three NH groups present in dipeptides **3–5** serves as an IHB donor in the β-turn structure.

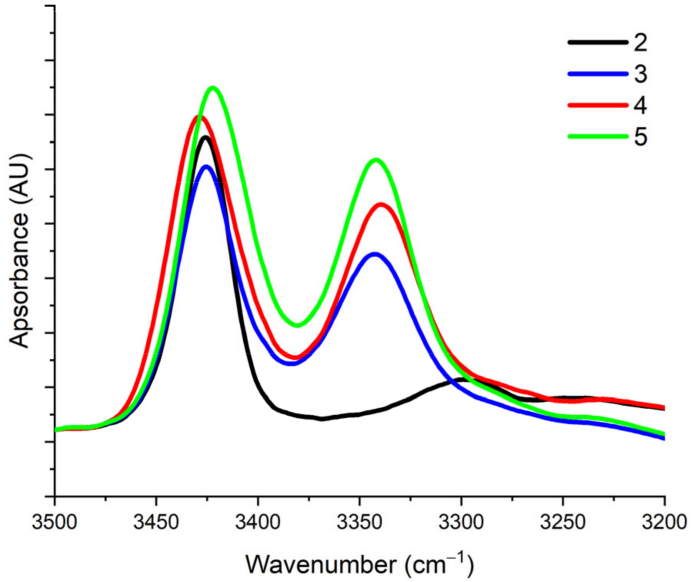

Figure 3. The NH stretching vibrations of **2–5** in CH_2Cl_2 ($c = 1{\cdot}10^{-3}$ mol dm^{-3}).

The carbonyl function of the *tert*-butyl ester in the amide I region of the spectra of **3–5** is centered below 1720 cm^{-1}, which indicates its involvement in IHBs [37,38]. Although the type of IHB pattern cannot be unambiguously determined from IR absorption data alone, these findings and the negligible intensity of the band below 3400 cm^{-1} in the spectrum

of **2** suggest the formation of a ten-membered $NH_{Fc}\cdots CO_{Boc}$ IHB ring in solutions of **3–5**. This assumption is consistent with the higher chemical shift values of NH_{Fc} resonances (d ~ 8.40 ppm) in the NMR spectra of dilute solutions (Figure S9) of **3–5** compared to **2** (d = 7.99 ppm). Moreover, diagnostic sequential d_{NN} (i, i + 1) and $d_{\alpha N}$ (i, i + 1) connectivities between NH_{Fc}-NH_{Ac6c}, NH_{Ac6c} − NH_{AA}, and NH_{Ac6c} − CH_{AA} (Figure 4) observed in the NOESY spectra of derivatives **3–5** (Figures S10–S12) suggest folding in the β-turn structure [39]. The chiral influence of the *N*-terminal amino acid is evident in the separation of the diasterotopic ferrocene protons in the spectra of compounds **3–5** compared to achiral **2**, in whose spectra they coalesce to a single signal (Figure 4). The anisochrony of these protons originates from the chiral environment experienced by ferrocene, caused by a dominant screw sense of turn structure in the peptide segment. In the absence of IHBs, even in chiral compounds, these signals are not resolved on the NMR time scale due to the fast rotation around single bonds [33].

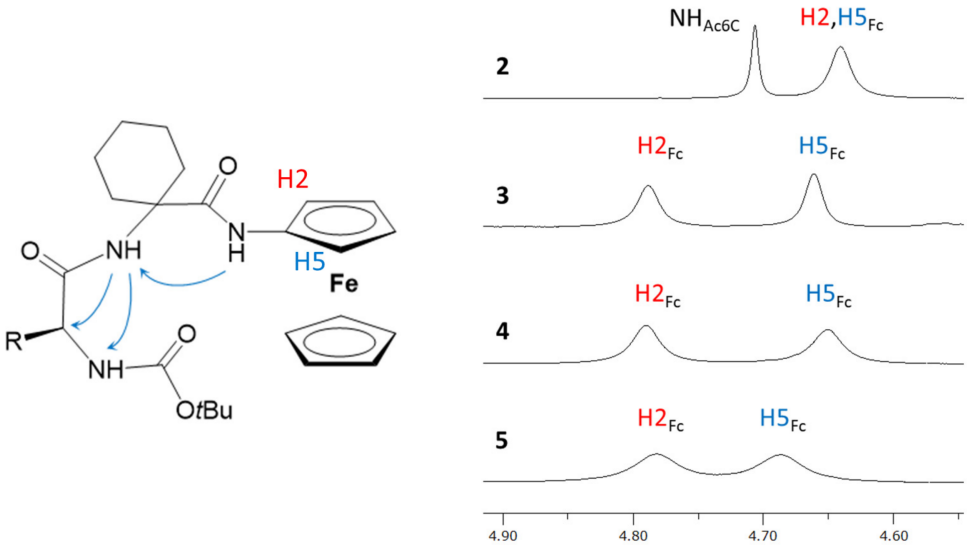

Figure 4. Sequential d_{NN} (i, i + 1) and $d_{\alpha N}$ (i, i + 1) NOEs in the spectra of **3–5** and portion of the ^{1}H NMR spectra of **2–5** showing the anisochronicity of diastereotopic ferrocene H2 and H5 protons.

2.2. CD Studies

Finally, to test whether the chiral *N*-terminal residue causes the folding of the peptide chain in a dominant direction, leading to an asymmetric distribution of conformers with different angle χ values and thus the chiroptical activity of the inherently achiral ferrocene chromophore, we recorded the CD spectra of derivatives **2–5**. As seen in Figure 5, the CD band in the spectrum of probe **2** is almost flat, while the introduction of L-amino acids gives rise to negative Cotton effects in the spectra of derivatives **3–5**. These results are consistent with our assumptions from the introduction: L-amino acids prefer the right-handed β-turn conformation, which, with *trans*-like orientation to ferrocene, causes a negative χ angle and thus a negative CD signal. Although experimental data indicate the predominance of the *trans*-like orientation of the peptide segment toward ferrocene in solutions of **3–5**, allowing a CD-signal-chirality correlation in the continuation of the research, we performed a density functional theory study (DFT) to obtain the distribution of low energy conformers.

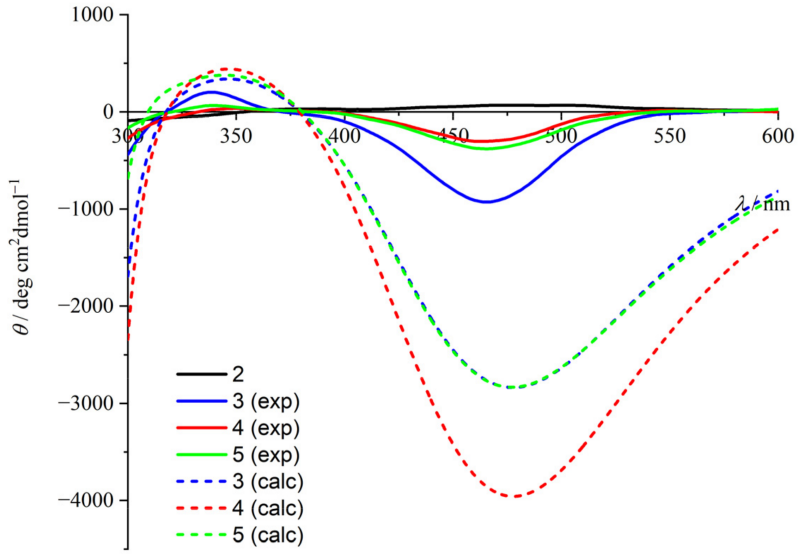

Figure 5. CD spectra of **2–5** in CH_2Cl_2 ($c = 1 \cdot 10^{-3}$ mol dm^{-3}).

2.3. Computational Studies

The hydrogen bonding patterns of the most stable conformers of **3–5** were studied using a three-step strategy, which we have already presented in our publications [22,25–27,29,40]. The initial geometries were optimized relatively quickly by molecular mechanics, and only the most stable conformers were further optimized at the B3LYP-D3 level in solvent treated as a polarizable continuum. The hydrogen bonds were confirmed by comparing the calculated Quantum theory of atoms in molecules (QTAIM) topological data with those proposed by Koch and Popelier [41].

For all three compounds, the final set of conformers consists of the very similar lowest energy structures (**3–1**, **4–1** and **5–1**), over 75% of which is populated with a single ten-membered ring (β-turn) connected by $NH_{Fc}\cdots OC_{Boc}$ IHB (Figure 5). Other energetically less stable conformers are characterized by one or two seven-membered rings connected by $NH_{Fc}\cdots OC_{AA}$ and/or $NH_{Ac6c}\cdots OC_{Boc}$ hydrogen bond(s). As expected, the sterically bulkier Ac6c amino acid influenced the final distribution of conformers more strongly than its acyclic analog Aib, i.e., the most stable conformers (**3–1**, **4–1**, and **5–1**) are not only much more populated than the following ones, but also preferentially form *trans*-like structures with the *P*-helical substituent pointing in the opposite direction to the second Cp ring of the ferrocene. In such an arrangement, the negative dihedral angles χ coincide well with the negative sign of calculated CD curves, as shown in Figure S13. In contrast, the positive dihedral angles χ in less favorable conformers coincide with the positive sign of the CD curves, but because of their lower abundance in the overall Boltzmann distribution, their contribution in the averaged calculated CD curves is less important (Figure 6). Although the intensity of the averaged calculated CD curves is higher than the experimentally measured ones, both have negative signs and the calculated CD curves agree almost perfectly with the experimental data. As described in previous papers [28,29], the amide group directly attached to the Cp ring can occupy different positions depending on the rotation around the C−N bond. Natural transition orbitals and density difference plots for the first six excited states of the most stable conformers in each series (Figures S14–S31) indicated that a local excitation influenced by different orientations of the attached amide plane relative to the Cp ring plane (described by the angle χ value) also perturbs the highly symmetric ferrocene, eventually leading to the predetermined sign of the CD signal near 470 nm. Carefully designed structural modifications, such as the substitution of acyclic Aib for cyclic Ac6c, affect the final distribution of conformers in a predicted manner by favoring *trans*-like conformers with a clearly defined relationship between the dihedral angle χ and the experimentally/computationally determined CD curves.

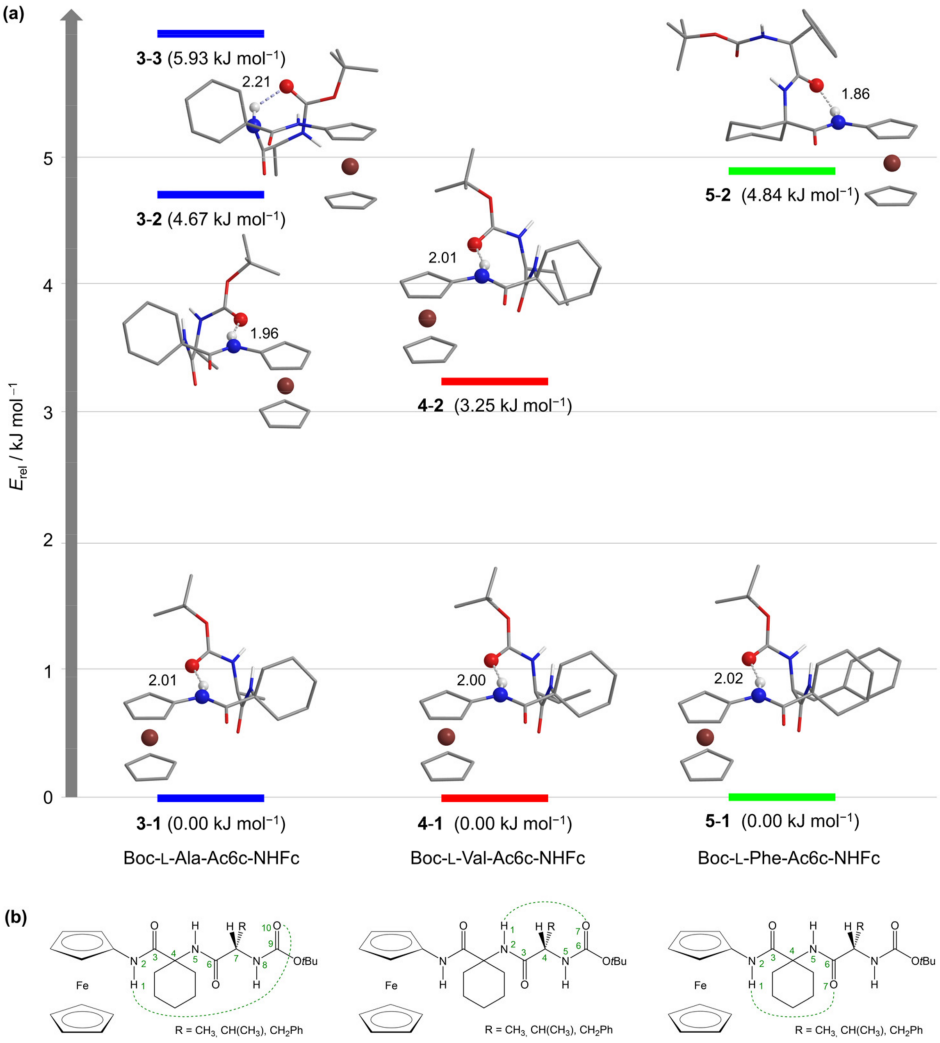

Figure 6. (**a**) The most stable conformers of **3–5**. (**b**) Intramolecular hydrogen bond patterns observed in **3–5**.

3. Materials and Methods

3.1. General

Commercial reagents, EDC [EDC = *N*-(3-dimethylaminopropyl)-*N*-ethylcarbodiimide hydrochloride, Acros Organics], HOBt (HOBt = 1-hydroxybenzotriazole, Merck, New Jersey), and Boc−Ac6c−OH (Merck) were used as received. *N*-Boc-protected L-AA (AA = Ala, Val, Phe) was prepared by the action of di-*tert*-butyldicarbonate in the presence of sodium hydroxide in aqueous dioxane. CH_2Cl_2 used for synthesis and spectroscopy was dried (P_2O_5), distilled from CaH_2, and stored over molecular sieves (4 Å). Products were purified by preparative thin-layer chromatography on silica gel (Merck, Kieselgel 60 HF254) using CH_2Cl_2/ethyl acetate mixtures as eluents. IR absorption spectra were recorded as $CHCl_3$ solutions using a Bomem MB 100 mid FTIR spectrophotometer. UV/Vis and CD spectra were recorded in CH_2Cl_2 using a Jasco-810 spectropolarimeter. NMR spectra were recorded at 600.130 MHz for ^1H and 150.903 MHz for ^{13}C using the Bruker Avance spectrometer with a 5 mm TBI probe at the Ruđer Bošković Institute.

*3.2. Synthesis of Boc−Ac6c−NH−Fc (**2**) and Boc−AA−Ac6c−NH−Fc (**3–5**)*

Boc−NH−Fc (**1**) or Boc−Ac6c−NH−Fc (**2**) (1 mmol) was deprotected by the action of gaseous HCl in dry CH_2Cl_2 (10 mL) at 0 °C for two hours. After evaporation of the solvent, the resulting hydrochloride was suspended in MeCN, treated with Et_3N (pH~8) and coupled with HOBt/EDC (2.2 mmol) activated Boc−AA−OH (2 mmol). The reaction

mixture was stirred for two hours at RT (**2**) or for 24 h at 65 °C (**3**–**5**) and evaporated to dryness. The residue was diluted with CH_2Cl_2, washed three times with saturated $NaHCO_3$ solution, 10% aqueous citric acid solution, brine, and dried over Na_2SO_4. After removing the solvent, the crude products were purified by preparative TLC on silica gel using mixtures of dichloromethane and ethyl acetate as eluents.

3.2.1. Boc–Ac6c–NH–Fc (**2**)

Yield 388 mg (91%), mp 130–131 °C. ^{1}H-NMR ($CDCl_3$, c = 0.1 mol dm^{-3}) δ/ppm: 8.27 (s, 1H, NH_{Fc}), 4.71 (s, 1H, NH_{Ac6c}), 4.64 (s, 2H, H-2, H-5), 4.17 (s, 5H, Fc), 4.0 (bs, 2H, H-3, H-4), 2.07–2.01 (m, 2H, $CH_2\beta_{Ac6c}$), 1.94–1.88 (m, 2H, $CH_2\beta_{Ac6c}$), 1.70–1.61 (m, 4H, $CH_2\gamma_{Ac6c}$), 1.49 (s, 9H, $C(CH_3)_3$), 1.45–1.31 (m, 2H, CH_2d_{Ac6c}). ^{13}C-NMR ($CDCl_3$, c = 0.1 mol dm^{-3}) δ/ppm: 172.7 (CO_{Ac6c}), 155.3 (CO_{Boc}), 95.1 (C-1), 80.5 (Cq_{Boc}), 69.3 (Cp), 64.5 (C-3, C-4), 61.2 (C-2, C-5), 59.7 ($C\alpha_{Ac6c}$), 32.1 ($CH_2\beta_{Ac6c}$), 29.7 ($CH_2\beta_{Ac6c}$), 28.3 (CH_{3Boc}), 25.2 (CH_2d_{Ac6c}), 21.3 ($CH_2\gamma_{Ac6c}$). Elemental analysis calcd for $C_{22}H_{30}N_2O_3Fe$: C 61.98, H 7.09, N 6.57, found: C 57.86, H 7.01, N 6.48. IR (CH_2Cl_2): ν_{max}/cm^{-1}: 3426 m (NHfree), 2976 sh, 2932 m, 2859 m (CH_2), 1722 s, 1694 s (amide I).

3.2.2. Boc–L–Ala–Ac6c–NH–Fc (**3**)

Yield 348 (79%), mp 98 °C. ^{1}H-NMR ($CDCl_3$, c = 0.1 mol dm^{-3}) δ/ppm: 8.43 (s, 1H, NH_{Fc}), 6.34 (s, 1H, NH_{Ac6c}), 5.00 (s, 1H, NH_{Ala}), 4.79 (s, 1H, H-2), 4.67 (s, 1H, H-5), 4.17 (s, 5H, Fc), 4.06 (m, 1H, $CH\alpha_{Ala}$), 3.99 (bs, 2H, H-3, H-4), 2.28–2.23 (s, 1H, $CH_2\beta_{Ac6c}$), 2.04–1.95 (m, 2H, $CH_2\beta_{Ac6c}$), 1.91–1.85 (m, 1H, $CH_2\beta_{Ac6c}$), 1.71–1.60 (m, 4H, $CH_2\gamma_{Ac6c}$), 1.49 (s, 9H, $C(CH_3)_3$), 1.40 (d, J = 6.6 Hz, 3H, CH_{3Ala}), 1.33–1.28 (m, 2H, CH_2d_{Ac6c}).^{13}C-NMR ($CDCl_3$, c = 0.1 mol dm^{-3}) δ/ppm: 172.3 (CO_{Ac6c}), 172.2 (CO_{Ala}), 156.2 (CO_{Boc}), 92.6 (C-1), 81.1 (Cq_{Boc}), 69.4 (Cp), 64.5 (C-3), 64.3 (C-4), 61.4 (C-2), 61.0 (C-5), 60.5 ($C\alpha_{Ac6c}$), 51.7 ($CH\alpha_{Ala}$), 33.0 ($CH_2\beta_{Ac6c}$), 30.9 ($CH_2\beta_{Ac6c}$), 28.3 (CH_{3Boc}), 25.1 (CH_2d_{Ac6c}), 21.4 ($CH_2\gamma_{Ac6c}$), 21.3 ($CH_2\gamma_{Ac6c}$), 17.4 (CH_{3Ala}). Elemental analysis calcd for $C_{25}H_{35}N_3O_4Fe$: C 60.37, H 7.09, N 8.45, found: C 60.29, H 7.05, N 8.51. IR (CH_2Cl_2): ν_{max}/cm^{-1}: 3425 m (NHfree), 3342 m (NHassoc.), 2935 m, 2860 m (CH_2), 1699 s (amide I).

3.2.3. Boc–L–Val–Ac6c–NH–Fc (**4**)

Yield 357 mg (68%), mp 102–103 °C. ^{1}H-NMR ($CDCl_3$, c = 0.1 mol dm^{-3}) δ/ppm: 8.48 (s, 1H, NH_{Fc}), 6.18 (s, 1H, NH_{Ac6c}), 4.98 (d, J = 5.4 Hz, 1H, NH_{Val}), 4.74 (s, 1H, H-2), 4.60 (s, 1H, H-5), 4.16 (s, 5H, Fc), 3.96 (bs, 2H, H-3, H-4), 3.82 (t, J = 6.0 Hz, 1H, $CH\alpha_{Val}$), 2.32–2.22 (m, 2H, $CH\beta_{Val}$, $CH_2\beta_{Ac6c}$), 2.04–1.96 (m, 2H, $CH_2\beta_{Ac6c}$), 1.93–1.86 (m, 1H, $CH_2\beta_{Ac6c}$), 1.73–1.60 (m, 4H, $CH_2\gamma_{Ac6c}$), 1.48 (s, 9H, $C(CH_3)_3$), 1.35–1.28 (m, 2H, CH_2d_{Ac6c}), 1.06 (d, J = 6.6 Hz, 3H, CH_{3Val}), 1.01 (d, J = 6.6 Hz, 3H, CH_{3Val}). ^{13}C-NMR ($CDCl_3$, c = 0.1 mol dm^{-3}) δ/ppm: 172.1 (CO_{Ac6c}), 171.6 (CO_{Val}), 156.5 (CO_{Boc}), 92.5 (C-1), 80.9 (Cq_{Boc}), 69.4 (Cp), 64.6 (C-3), 64.3 (C-4), 61.6 (C-2), 61.4 (C-5), 61.0 ($CH\alpha_{Val}$), 60.9 ($C\alpha_{Ac6c}$), 52.1 ($CH\alpha_{Val}$), 33.3 ($CH_2\beta_{Ac6c}$), 30.9 ($CH_2\beta_{Ac6c}$), 29.7 ($CH\beta_{Val}$), 28.6 (CH_{3Boc}), 25.1 (CH_2d_{Ac6c}), 21.4 ($CH_2\gamma_{Ac6c}$), 21.3 ($CH_2\gamma_{Ac6c}$), 19.6 (CH_{3Val}), 18.0 (CH_{3Val}). Elemental analysis calcd for $C_{27}H_{39}N_3O_4Fe$: C 61.72, H 7.48, N 8.0, found: C 61.80, H 7.45, N 8.05. IR (CH_2Cl_2): ν_{max}/cm^{-1}: 3429 m (NHfree), 3340 m (NHassoc.), 2976 sh, 2932 m, 2858 m (CH_2), 1702 m (amide I).

3.2.4. Boc–L–Phe–Ac6c–NH–Fc (**5**)

Yield 413 mg (72%), mp 113 °C. ^{1}H-NMR ($CDCl_3$, c = 0.1 mol dm^{-3}) δ/ppm: 8.38 (s, 1H, NH_{Fc}), 7.35–7.32 (m, 2H, $CH\gamma_{Phe}$), 7.29–7.27 (m, 1H, CHd_{Phe}), 7.25–7.23 (m, 2H, $CH\beta_{Phe}$), 6.09 (s, 1H, NH_{Ac6c}), 4.99 (bs, 1H, NH_{Phe}), 4.72 (s, 1H, H-2), 4.69 (s, 1H, H-5), 4.25–4.20 (m, 1H, $CH\alpha_{Phe}$), 4.19 (s, 5H, Fc), 4.00 (bs, 2H, H-3, H-4), 3.24–3.19 (m, 1H, $CH_2\beta_{Phe}$), 3.06–3.01 (m, 1H, $CH_2\beta_{Phe}$), 2.15–2.10 (m, 1H, $CH_2\beta_{Ac6c}$), 2.00–1.94 (m, 2H, $CH_2\beta_{Ac6c}$), 1.91–1.85 (m, 1H, $CH_2\beta_{Ac6c}$), 1.68–1.53 (m, 4H, $CH_2\gamma_{Ac6c}$), 1.45 (s, 9H, $C(CH_3)_3$), 1.30–1.19 (m, 2H, CH_2d_{Ac6c}). ^{13}C-NMR ($CDCl_3$, c = 0.1 mol dm^{-3}) δ/ ppm: 171.9 (CO_{Ac6c}), 171.0 (CO_{Phe}), 156.1 (CO_{Boc}), 136.3 (CαPhe), 129.1 (CβPhe), 129.0 (CγPhe), 127.3 (CdPhe), 94.7 (C-1), 81.2 (Cq_{Boc}), 69.4 (Cp), 64.5 (C-3), 64.3 (C-4), 61.3 (C-2), 61.1 (C-5), 60.8 ($C\alpha_{Ac6c}$), 57.2

($CH\alpha_{Phe}$), 37.2 ($CH_2\beta_{Phe}$), 32.1 ($CH_2\beta_{Ac6c}$), 29.7 ($CH_2\beta_{Ac6c}$), 28.2 (CH_{3Boc}), 25.2 (CH_2d_{Ac6c}), 21.3 ($CH_2\gamma_{Ac6C}$). Elemental analysis calcd for $C_{31}H_{39}N_3O_4Fe$: C 64.92, H 6.85, N 7.33 found: C 64.98, H 6.79, N 7.29. IR (CH_2Cl_2): ν_{max}/cm^{-1}: 3422 m (NHfree), 3342 m (NHassoc.), 2930 m, 2858 m (CH_2), 1710 m (amide I).

3.3. Computational Details

For each series of compounds (**3**–**5**), the conformational search was performed in three steps. The first step included Monte Carlo Multiple Minimum and Mixed torsional/Low-mode sampling with molecular mechanics (OPLS2005 force field) in MacroModel [42,43]. A few hundred of the most stable geometries were selected for further optimizations at a high level of theory and run in Gaussian16 [44] with a default grid and convergence criteria. All calculations were performed at the B3LYP/ Lanl2DZ, and only the most stable conformers at the B3LYP/6-311+G(d,p) (LanL2DZ basis set on Fe) level of theory while surrounding the solvent (chloroform) was described as a polarizable continuum (SMD) [45]. Each optimized geometry was verified as a true minimum on the potential energy surface by vibrational analysis. Reported energies refer to standard Gibbs free energies at 298 K. Excited-state calculations were run with the TD-DFT method at the same level of theory used for the optimization of conformers. Average CD spectra were calculated by weighting CD spectra calculated for each conformer (from the ensemble of the most stable conformers) with Boltzmann factors at 298 K. Natural transition orbitals and density difference plots were visualized in GaussView6 [46]. Displayed hydrogen bonds were characterized using the QTAIM theory and analyzed with AIMAll [46]. Topological parameters of the displayed bond critical points between hydrogen bond acceptors and hydrogen atoms were calculated and verified according to the Koch and Popelier criteria [47].

4. Conclusions

Using three new compounds (Boc−AA−Ac6c−NH−Fc; AA = L-Ala, L-Val, L-Phe) derived from the monosubstituted aminoferrocene, we have investigated the effect of the incorporated achiral 1-aminocyclohexanecarboxylic acid (Ac6c) on the transfer of chiral information from three different L-amino acids to the ferrocene chromophore. The amino acid attached to the *N*-terminus causes a folding of the dipeptide sequence, in which ten-membered or seven-membered rings connect the potential hydrogen bond donors and hydrogen bond acceptors. Through a joint experimental and computational approach, we confirmed that the binding of the more sterically demanding Ac6c amino acid directly to the aminoferrocene core represents another step in the development of a practical ferrocene-based circular dichroism sensor for determining the chirality of amino acids and small helical peptide structures. Compared to its acyclic analog, α-amino isobutyric acid (Aib), which has relatively closely distributed conformers and is Ac6c attached to the single L-amino acid (such as Ala, Val, or Phe), mostly forms the *trans*-like configuration with the *P*-helical substituent and the ferrocene group in opposite directions to each other. With such an arrangement of the two groups, based on the value of the dihedral angle χ describing the relative position of the amide and the Cp plane, the sign of the CD signal of the perturbed ferrocene chromophore near 470 nm also changes in the predicted manner. Together with the fact that the adsorption region of the perturbed ferrocene chromophore does not overlap with the adsorption maxima of common solvents and other organic chromophores, it seems very reasonable to explore the possible application of Ac6c−NH−Fc as a chiroptical sensor in future studies.

Supplementary Materials: The following supporting information can be downloaded at: https://www.mdpi.com/article/10.3390/inorganics11060225/s1, Figure S1: ^{1}H NMR spectrum of **2**, full range; Figure S2: ^{13}C NMR spectrum of 2, full range; Figure S3: ^{1}H NMR spectrum of **3**, full range; Figure S4: ^{13}C NMR spectrum of **3**, full range; Figure S5: ^{1}H NMR spectrum of **4**, full range; Figure S6: ^{13}C NMR spectrum of **4**, full range; Figure S7: ^{1}H NMR spectrum of **5**, full range; Figure S8: ^{13}C NMR spectrum of 5, full range; Figure S9. NH_{Fc} resonances in the NMR spectra of dilute solutions of **2**–**5** (c = 2 mmol dm^{-3}); Figure S10. Sequential interactions in the NOESY spectrum of **3**; Figure S11. Sequential interactions in the NOESY

spectrum of **4**; Figure S12. Sequential interactions in the NOESY spectrum of **5**; Figure S13. TD-DFT calculated ECD spectra of **3**, **4** and **5**. The final Boltzmann-averaged spectrum at 298 K (red dashed line) is obtained by weighting each conformer spectrum (colored solid lines) with the appropriate conformer Boltzmann weight factor for the final set of structures as named in Table S1; Figure S14. Excited state **1** of the conformer **3–1**; Figure S15. Excited state **2** of the conformer **3–1**; Figure S16. Excited state **3** of the conformer **3–1**; Figure S17. Excited state **4** of the conformer **3–1**; Figure S18. Excited state 5 of the conformer 3–1; Figure S19. Excited state 6 of the conformer 3–1; Figure S20. Excited state 1 of the conformer **4–1**; Figure S21. Excited state **2** of the conformer **4–1**; Figure S22. Excited state **3** of the conformer **4–1**; Figure S23. Excited state **4** of the conformer **4–1**; Figure S24. Excited state **5** of the conformer **4–1**; Figure S25. Excited state **6** of the conformer **4–1**; Figure S26. Excited state **1** of the conformer **5–1**; Figure S27. Excited state **2** of the conformer **5–1**; Figure S28. Excited state **3** of the conformer **5–1**; Figure S29. Excited state **4** of the conformer **5–1**; Figure S30. Excited state **5** of the conformer **5–1**; Figure S31. Excited state **6** of the conformer **5–1**; Table S1: Relative energies (in kJ mol^{-1}) of the most stable conformers (<10 kJ mol^{-1}) of compounds **3–5** optimized in chloroform at 298 K. Optimizations performed at the B3LYP-D3/6-311+G(d,p), LanL2DZ for Fe level of theory, SMD model for solvent effects. Value of the χ angle (in deg), X–Y distances (in Å) of the selected X−H·Y hydrogen bonds connecting the *n*-membered rings; Figure S32: UV/Vis spectra of compounds **2–5**.

Author Contributions: Conceptualization, M.Č.S. and I.K.; methodology, M.Č.S. and I.K.; software, I.K.; investigation, M.N., M.K., P.Š., I.K. and M.Č.S.; writing—original draft preparation, M.N., M.K., I.K. and M.Č.S.; writing—review and editing, M.Č.S. and I.K. All authors have read and agreed to the published version of the manuscript.

Funding: This work has been fully supported by the Croatian Science Foundation under the project IP-2020-02-9162.

Data Availability Statement: The DFT and spectroscopic data are included in the paper and supplementary materials.

Acknowledgments: We want to thank the Croatian Academy of Sciences and Arts for the financial support given to I.K. for the computational studies.

Conflicts of Interest: The authors declare no conflict of interest.

References

1. Ozcelik, A.; Pereira-Cameselle, R.; Poklar Ulrih, N.; Petrovic, A.G.; Alonso-Gómez, J.L. Chiroptical Sensing: A Conceptual Introduction. *Sensors* **2020**, *20*, 974. [CrossRef]
2. Saito, F.; Schreiner, P.R. Determination of the Absolute Configurations of Chiral Alkanes—An Analysis of the Available Tools. *Eur. J. Org. Chem.* **2020**, *2020*, 6328–6339. [CrossRef]
3. Herrera, B.T.; Pilicer, S.L.; Anslyn, E.V.; Joyce, L.A.; Wolf, C. Optical Analysis of Reaction Yield and Enantiomeric Excess: A New Paradigm Ready for Prime Time. *J. Am. Chem. Soc.* **2018**, *140*, 10385–10401. [CrossRef] [PubMed]
4. Yang, L.; Luoa, L.; Wei, W. Simultaneous determination of the concentration and enantiomeric excess of amino acids with a coumarin-derived achiral probe. *Anal. Methods* **2021**, *13*, 1905–1910. [CrossRef] [PubMed]
5. Ni, C.; Zha, D.; Ye, H.; Hai, Y.; Zhou, Y.; Anslyn, E.V.; You, L. Dynamic covalent chemistry within biphenyl scaffolds: Reversible covalent bonding, control of selectivity, and chirality sensing with a single system. *Angew. Chem. Int. Ed.* **2018**, *57*, 1300–1305. [CrossRef]
6. Zong, Z.; Cao, Z.; Hao, A.; Xing, P. Dynamic axial chirality of ferrocene diamino acids: Hydration effects and chiroptical applications. *J. Mater. Chem. C* **2021**, *9*, 12191–12200. [CrossRef]
7. Thanzeel, F.Y.; Sripada, A.; Wolf, C. Quantitative Chiroptical Sensing of Free Amino Acids, Biothiols, Amines, and Amino Alcohols with an Aryl Fluoride Probe. *J. Am. Chem. Soc.* **2019**, *141*, 16382–16387. [CrossRef]
8. Thanzeel, F.Y.; Zandia, L.S.; Wolf, C. Chiroptical sensing of homocysteine. *Org. Biomol. Chem.* **2020**, *18*, 8629–8632. [CrossRef]
9. Thanzeel, F.Y.; Balaraman, K.; Wolf, C. Quantitative Chirality and Concentration Sensing of Alcohols, Diols, Hydroxy Acids, Amines and Amino Alcohols using Chlorophosphite Sensors in a Relay Assay. *Angew. Chem. Int. Ed.* **2020**, *59*, 21382–21386. [CrossRef]
10. De los Santos, Z.A.; Wolf, C. Optical Terpene and Terpenoid Sensing: Chiral Recognition, Determination of Enantiomeric Composition and Total Concentration Analysis with Late Transition Metal Complexes. *J. Am. Chem. Soc.* **2020**, *142*, 4121–4125. [CrossRef]
11. Hassan, D.S.; Thanzeel, F.Y.; Wolf, C. Stereochemical analysis of chiral amines, diamines, and amino alcohols: Practical chiroptical sensing based on dynamic covalent chemistry. *Chirality* **2020**, *32*, 457–463. [CrossRef] [PubMed]

12. Lynch, C.C.; De los Santos, Z.A.; Wolf, C. Chiroptical sensing of unprotected amino acids, hydroxy acids, amino alcohols, amines and carboxylic acids with metal salts. *Chem. Commun.* **2019**, *55*, 6297–6300. [CrossRef]
13. De los Santos, Z.A.; Lynch, C.C.; Wolf, C. Dynamic Covalent Optical Chirality Sensing with a Sterically Encumbered Aminoborane. *Chem. Eur. J.* **2022**, *28*, e202202028. [CrossRef] [PubMed]
14. Hassan, D.S.; De los Santos, Z.A.; Brady, K.G.; Murkli, S.; Isaacs, L.; Wolf, C. Chiroptical sensing of amino acids, amines, amino alcohols, alcohols and terpenes with π-extended acyclic cucurbiturils. *Org. Biomol. Chem.* **2021**, *19*, 4248–4253. [CrossRef] [PubMed]
15. Formen, J.S.S.K.; Wolf, C. Chiroptical Switching and Quantitative Chirality Sensing with (Pseudo)halogenated Quinones. *Angew. Chem. Int. Ed.* **2021**, *60*, 27031–27038. [CrossRef] [PubMed]
16. Astruc, D. Why is Ferrocene so Exceptional? *Eur. J. Inorg. Chem.* **2017**, *2017*, 6–29. [CrossRef]
17. Patti, A.; Pedotti, S.; Mazzeo, G.; Longhi, G.; Abbate, S.; Paoloni, L.; Bloino, J.; Rampino, S.; Barone, V. Ferrocenes with simple chiral substituents: An in-depth theoretical and experimental VCD and ECD study. *Phys. Chem. Chem. Phys.* **2019**, *21*, 9419–9432. [CrossRef]
18. Brahma, S.; Ikbal, S.S.; Dhamija, A.; Prasad Rath, S. Highly Enhanced Bisignate Circular Dichroism of Ferrocene-Bridged Zn(II) Bisporphyrin Tweezer with Extended Chiral Substrates due to Well-Matched Host–Guest System. *Inorg. Chem.* **2014**, *53*, 2381–2395. [CrossRef]
19. Adhikari, B.; Kraatz, H.-B. Redox-triggered changes in the self-assembly of a ferrocene–peptide conjugate. *Chem. Commun.* **2014**, *50*, 5551–5553. [CrossRef]
20. Moriuchi, T.; Hirao, T. Dipeptide-induced chirality organization. *J. Incl. Phenom. Macrocycl. Chem.* **2012**, *74*, 23–40. [CrossRef]
21. Kirin, S.I.; Wissenbach, D.; Metzler-Nolte, N. Unsymmetrical 1,n′-disubstituted ferrocenoyl peptides: Convenient one pot synthesis and solution structures by CD and NMR spectroscopy. *New J. Chem.* **2005**, *29*, 1168–1173. [CrossRef]
22. Kovačević, M.; Kodrin, I.; Cetina, M.; Kmetič, I.; Murati, T.; Čakić Semenčić, M.; Roca, S.; Barišić, L. The conjugates of ferrocene-1,1′-diamine and amino acids. A novel synthetic approach and conformational analysis. *Dalton Trans.* **2015**, *44*, 16405–16420. [CrossRef] [PubMed]
23. Čakić Semenčić, M.; Siebler, D.; Heinze, K.; Rapić, V. Bis- and Trisamides Derived From 1′-Aminoferrocene-1-carboxylic Acid and α-Amino Acids: Synthesis and Conformational Analysis. *Organometallics* **2009**, *28*, 2028–2037. [CrossRef]
24. Herrick, R.S.; Jarret, R.M.; Curran, T.P.; Dragoli, D.R.; Flaherty, M.B.; Lindyberg, S.E.; Slate, R.A.; Thornton, L.C. Ordered conformations in bis(amino acid) derivatives of 1,1′-ferrocenedicarboxylic acid. *Tetrahedron Lett.* **1996**, *37*, 5289–5292. [CrossRef]
25. Kovač, V.; Čakić Semenčić, M.; Kodrin, I.; Roca, S.; Rapić, V. Ferrocene-dipeptide conjugates derived from aminoferrocene and 1-acetyl-1′-aminoferrocene: Synthesis and conformational studies. *Tetrahedron* **2013**, *69*, 10497–10506. [CrossRef]
26. Čakić Semenčić, M.; Kodrin, I.; Barišić, L.; Nuskol, M.; Meden, A. Synthesis and Conformational Study of Monosubstituted Aminoferrocene- Based Peptides Bearing Homo-and Heterochiral Pro-Ala Sequences. *Eur. J. Inorg. Chem.* **2017**, *2017*, 306–317. [CrossRef]
27. Nuskol, M.; Studen, B.; Meden, A.; Kodrin, I.; Čakić Semenčić, M. Tight Turn in Dipeptide Bridged Ferrocenes: Synthesis, X-Ray Structural, Theoretical and Spectroscopic Studies. *Polyhedron* **2019**, *161*, 137–144. [CrossRef]
28. Nuskol, M.; Šutalo, P.; Đaković, M.; Kovačević, M.; Kodrin, I.; Čakić Semenčić, M. Testing the Potential of the Ferrocene Chromophore as a Circular Dichroism Probe for the Assignment of the Screw-Sense Preference of Tripeptides. *Organometallics* **2021**, *40*, 1351–1362. [CrossRef]
29. Nuskol, M.; Šutalo, P.; Kodrin, I.; Čakić Semenčić, M. Sensing of the Induced Helical Chirality by the Chiroptical Response of the Ferrocene Chromophore. *Eur. J. Inorg. Chem.* **2022**, *2022*, e202100880. [CrossRef]
30. Venkatraman, J.; Shankaramma, S.C.; Balaram, P. Design of folded peptides. *Chem. Rev.* **2001**, *101*, 3131–3152. [CrossRef]
31. Clayden, J.; Castellanos, A.; Solà, J.; Morris, G.A. Quantifying End-to-End Conformational Communication of Chirality through an Achiral Peptide Chain. *Angew. Chem. Int. Ed.* **2009**, *48*, 5962–5965. [CrossRef] [PubMed]
32. Toniolo, C.; Crisma, M.; Formaggio, F.; Peggion, C. Control of peptide conformation by the Thorpe-Ingold effect (C alpha-tetrasubstitution). *Biopolymers* **2001**, *60*, 396–419. [CrossRef] [PubMed]
33. Barišić, L.; Čakić, M.; Mahmoud, K.A.; Liu, Y.-N.; Kraatz, H.-B.; Pritzkow, H.; Kirin, S.I.; Metzler-Nolte, N.; Rapić, V. Helically Chiral Ferrocene Peptides Containing 1′-Aminoferrocene-1-Carboxylic Acid Subunits as Turn Inducers. *Chem. Eur. J.* **2006**, *12*, 4965–4980. [CrossRef]
34. Hirata, T.; Ueda, A.; Oba, M.; Doi, M.; Demizu, Y.; Kurihara, M.; Nagano, M.; Suemune, H.; Tanaka, M. Amino equatorial effect of a six-membered ring amino acid on its peptide 310- and α-helices. *Tetrahedron* **2015**, *71*, 2409–2420. [CrossRef]
35. Doi, M.; Asano, A.; Komura, E.; Ueda, Y. The structure of an endomorphin analogue incorporating 1-aminocyclohexane-1-carboxlylic acid for proline is similar to the β-turn of Leu-enkephalin. *Biochemical. Biophysical. Res. Commun.* **2002**, *297*, 138–142. [CrossRef]
36. Fabiano, N.; Valle, G.; Crisma, M.; Toniolo, C.; Saviano, M.; Lombardi, A.; Isernia, C.; Pavone, V.; Di Blasio, B.; Pedone, C.; et al. Conformational versatility of the Nα-acylated tripeptide amide tail of oxytocin. *Int. J. Pept. Protein Res.* **1993**, *42*, 459–465. [CrossRef] [PubMed]
37. Ananthanarayanan, V.S.; Cameron, T.S. Proline-containing β-turns. *Int. J. Pept. Protein Res.* **1988**, *31*, 399–411. [CrossRef] [PubMed]

38. Ganesh, S.; Jayakumar, R. Role of N-t-Boc group in helix initiation in a novel tetrapeptide. *J. Pept. Res.* **2002**, *59*, 249–256. [CrossRef]
39. Wuthrich, K. *NMR of Proteins and Nucleic Acids*; Wiley: New York, NY, USA, 1986.
40. Kovačević, M.; Čakić Semenčić, M.; Kodrin, I.; Roca, S.; Perica, J.; Mrvčić, J.; Stanzer, D.; Molčanov, K.; Milašinvić, V.; Brkljačić, L.; et al. Biological Evaluation and Conformational Preferences of Ferrocene Dipeptides with Hydrophobic Amino Acids. *Inorganics* **2023**, *11*, 29. [CrossRef]
41. Koch, U.; Popelier, P.L.A. Characterization of C-H-O Hydrogen Bonds on the Basis of the Charge Density. *J. Phys. Chem.* **1995**, *99*, 9747–9754. [CrossRef]
42. Schrödinger LLC. *MacroModel*; Schrödinger LLC: New York, NY, USA, 2019.
43. Mohamadi, F.; Richards, N.G.J.; Guida, W.C.; Liskamp, R.; Lipton, M.; Caufield, C.; Chang, G.; Hendrickson, T.; Still, W.C. Macromodel—An integrated software system for modeling organic and bioorganic molecules using molecular mechanics. *J. Comput. Chem.* **1990**, *11*, 440–467. [CrossRef]
44. Frisch, M.J.; Trucks, G.W.; Schlegel, H.B.; Scuseria, G.E.; Robb, M.A.; Cheeseman, J.R.; Scalmani, G.; Barone, V.; Petersson, G.A.; Nakatsuji, H.; et al. *Gaussian 16, Revision, C.01*; Gaussian, Inc.: Wallingford, CT, USA, 2016.
45. Marenich, A.V.; Cramer, C.J.; Truhlar, D.G. Universal Solvation Model Based on Solute Electron Density and on a Continuum Model of the Solvent Defined by the Bulk Dielectric Constant and Atomic Surface Tensions. *J. Phys. Chem. B* **2009**, *113*, 6378–6396. [CrossRef] [PubMed]
46. Dennington, R.; Keith, T.A.; Millam, J.M. *GaussView*, Version 6.1; Semichem Inc.: Shawnee Mission, KS, USA, 2016.
47. Keith, T.A. *AIMAll*; Version 19.02.13; TK Gristmill Software: Overland Park, KS, USA, 2017.